

## Non-Abelian SU(2) Lattice Gauge Theories in Superconducting Circuits

A. Mezzacapo,<sup>1,2</sup> E. Rico,<sup>1,3</sup> C. Sabín,<sup>4</sup> I. L. Egusquiza,<sup>5</sup> L. Lamata,<sup>1</sup> and E. Solano<sup>1,3</sup>

<sup>1</sup>*Department of Physical Chemistry, University of the Basque Country UPV/EHU, Apartado 644, 48080 Bilbao, Spain*

<sup>2</sup>*IBM T.J. Watson Research Center, Yorktown Heights, New York 10598, USA*

<sup>3</sup>*IKERBASQUE, Basque Foundation for Science, Maria Diaz de Haro 3, 48013 Bilbao, Spain*

<sup>4</sup>*School of Mathematical Sciences, University of Nottingham, Nottingham NG7 2RD, United Kingdom*

<sup>5</sup>*Department of Theoretical Physics and History of Science, University of the Basque Country UPV/EHU, Apartado 644, 48080 Bilbao, Spain*

(Received 26 May 2015; published 9 December 2015)

We propose a digital quantum simulator of non-Abelian pure-gauge models with a superconducting circuit setup. Within the framework of quantum link models, we build a minimal instance of a pure SU(2) gauge theory, using triangular plaquettes involving geometric frustration. This realization is the least demanding, in terms of quantum simulation resources, of a non-Abelian gauge dynamics. We present two superconducting architectures that can host the quantum simulation, estimating the requirements needed to run possible experiments. The proposal establishes a path to the experimental simulation of non-Abelian physics with solid-state quantum platforms.

DOI: [10.1103/PhysRevLett.115.240502](https://doi.org/10.1103/PhysRevLett.115.240502)

PACS numbers: 03.67.Ac, 03.67.Lx, 11.15.Ha, 85.25.Cp

Gauge invariance is a central concept in modern physics, being at the core of the standard model of elementary particle physics. In particular, invariances with respect to SU(2) and SU(3) gauge symmetries characterize the weak interaction and quantum chromodynamics [1,2]. In this sense, gauge theories represent a cornerstone in our understanding of the physical world and lie at the heart of diverse phenomena, such as the quark-gluon plasma or quantum spin liquids. In condensed matter physics, SU(2) gauge fields can also emerge dynamically in relation to exotic many-body phenomena, like quantum Hall systems, frustrated magnets, or superconductors [3–5].

Lattice gauge theories (LGT) are nonperturbative discrete formulations that contribute to the analysis of key features of these models, such as color confinement or chiral symmetry breaking. Starting from the seminal work by Wilson in 1974 [6,7], LGT have attracted a significant attention across several branches of theoretical physics. In the last decades [8], quantum Monte Carlo simulations have achieved unprecedented accuracies in determining the whole hadronic spectrum of the standard model. However, understanding its full phase diagram from first principles, or simulating dynamical processes, remains out of reach of current numerical computations.

Quantum simulators [9] provide a new approach to solve complex long-standing problems in quantum physics. In a quantum simulator, a proper encoding of LGT can allow for the retrieval of information about ground state and dynamics, in a wide range of regimes. Previous works have considered Abelian [10–22] and non-Abelian LGT in optical lattices [23–25] (see also Refs. [26,27] and references therein), both as analog and digital simulations [28]. In these implementations, matter-gauge interactions are modeled as a second-order process from Hubbard-like

interactions, while the simulation of pure-gauge dynamics remains more demanding.

In the last years, superconducting circuits have proven to be reliable devices that can host quantum information and simulation processes [29]. The possibility to perform quantum gates with high fidelities, together with high coherence times, makes them ideal devices for the realization of digital quantum simulations [30–34], previously considered in ion-trap systems [35–37].

In this Letter, we propose a digital quantum simulation of a non-Abelian dynamical SU(2) gauge theory in a superconducting device. We start by building a minimal setup, based on a triangular lattice, that can encode pure-gauge dynamics. The degrees of freedom of a single triangular plaquette of this lattice are encoded into qubits. We propose two implementations of this quantum simulator, using two different superconducting circuit architectures, as depicted in Fig. 1. We consider a setup in which six tunable-coupling transmon qubits are coupled to a single microwave resonator, and a device where six capacitively coupled Xmon qubits stand on a triangular geometry, coupled to a central auxiliary one. We compute experimental requirements necessary to perform the simulation on one plaquette, and provide arguments for scaling to large lattices.

*Lattice gauge theories.*—LGT are discretized versions of a gauge theory. In a conventional approach of lattice gauge theories, space-time is discretized while ensuring a covariant formulation of the theory. In quantum simulations, there is no direct access to the time direction, which is fixed and continuous. Hence, the equivalent Hamiltonian formulation of lattice models is used. In this case, the space is discretized and the action of a local gauge invariant Hamiltonian characterizes a continuous dynamical evolution. This fictitious asymmetry of the time direction forces us to define a

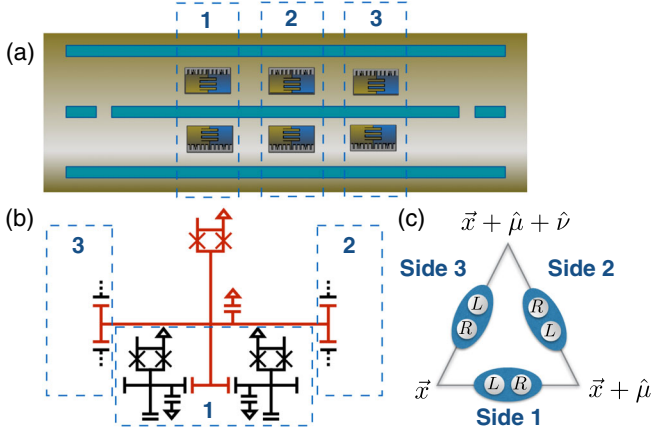


FIG. 1 (color online). (a) Six tunable-coupling transmon qubits coupled to a single microwave resonator. (b) Six Xmon qubits on a triangular geometry, coupled to a central one. The box 1 in the scheme is implicitly repeated for the sides 2 and 3. Both setups can encode the dynamics of the  $SU(2)$  triangular plaquette model schematized in (c), where the left and right gauge degrees of freedom are explicitly depicted.

physical Hilbert space or Gauss law of the model. We make use of a set of discretized space points  $\vec{x}$ , and  $SU(N)$  operators  $u(\vec{x}, \hat{\mu})$  associated to each link, connecting two adjacent sites  $(\vec{x}, \vec{x} + \hat{\mu})$ . A single  $u(\vec{x}, \hat{\mu})$  operator has two implicit color indices  $(\alpha, \beta)$ ,  $u_{\alpha\beta}$ , that connect the  $\alpha$ th component of the fermionic field at position  $\vec{x}$  with the  $\beta$ th component of the field at position  $\vec{x} + \hat{\mu}$ .

In order to construct a non-Abelian  $SU(N)$  theory built out of these  $u(\vec{x}, \hat{\mu})$  operators, one has to build a Hamiltonian that is invariant under a generic gauge transformation

$$u(\vec{x}, \hat{\mu}) \rightarrow e^{i\theta^a(\vec{x})\tau^a} u(\vec{x}, \hat{\mu}) e^{-i\theta^a(\vec{x}+\hat{\mu})\tau^a}, \quad (1)$$

where  $\tau^a$  are the  $(N^2 - 1)$  generators of the  $SU(N)$  algebra in the corresponding representation, and  $\theta^a$  the relative phase angles. It is straightforward to verify that the following Hamiltonian on a square lattice is gauge invariant

$$H = J \sum_{\vec{x}} \text{Tr} [u(\vec{x}, \hat{\mu}) u(\vec{x} + \hat{\mu}, \hat{\nu}) u^\dagger(\vec{x} + \hat{\nu}, \hat{\mu}) u^\dagger(\vec{x}, \hat{\nu})] + \text{H.c.}, \quad (2)$$

where the trace is performed over the color indices,  $J$  has energy units, and the directions  $\hat{\mu}$  and  $\hat{\nu}$  span the two-dimensional lattice. This Hamiltonian is a pure gauge operator, as it does not involve any fermionic operator and it is the minimum instance of a *Wilson loop* around a plaquette [1,2].

We focus now on the construction of a non-Abelian  $SU(2)$  quantum link model that mimics this gauge-invariant behavior in a finite-dimensional Hilbert space, suitable for quantum simulations. Notice that the framework of the quantum link models is valid for any compact Lie group [38]. We use a four-dimensional Hilbert space or,

equivalently, two qubits associated with each link. One can define link operators  $U(\vec{x}, \hat{\mu})$  acting on this four-dimensional Hilbert space with the associated gauge generators  $G^a(\vec{x})$  that satisfy the  $SU(2)$  algebra

$$[G^a(\vec{x}), G^b(\vec{y})] = i\delta_{\vec{x}\vec{y}} \sum_c \epsilon_{abc} G^c(\vec{x}). \quad (3)$$

To define the set of operators, we use a quantum link formulation [38], where the Hilbert space of a link is given by a set of bosonic modes  $c_{\alpha j}(\vec{x}, \hat{\mu})$  that implement the Schwinger representation of the  $SU(2)$  algebra, with  $\alpha \in \{\uparrow, \downarrow\}$ , acting on two different sites  $j \in \{L, R\}$  on the link between the two adjacent vertices  $\vec{x}$  and  $\vec{x} + \hat{\mu}$ . In this space, we build two sets of *right* and *left* generators  $R^a, L^a$ , on this finite-dimensional Hilbert space, using the bosonic modes  $c_{\alpha j}(\vec{x}, \hat{\mu})$  [39]. We define the gauge generators as  $G^a(\vec{x}) = \sum_{|\hat{\nu}|} L^a(\vec{x}, \hat{\nu}) + R^a(\vec{x} - \hat{\nu}, \hat{\nu})$ , where the sum over  $|\hat{\nu}|$  is taken among all the links of the lattice converging to a single vertex  $\vec{x}$ .

The representations of  $SU(2)$  are quasireal, therefore, ordinary and their dual representations (i.e., particle and antiparticle) are equivalent. Therefore, there are two multiplets with well-defined  $SU(2)$  transformations [39]. One can finally define the link operators, acting on the finite-dimensional Hilbert space of one link, in terms of Schwinger bosons on a given link [47–49],

$$U_{\alpha\beta} = \begin{pmatrix} c_{\uparrow L} & -ic_{\downarrow L}^\dagger \\ c_{\downarrow L} & ic_{\uparrow L}^\dagger \end{pmatrix} \begin{pmatrix} c_{\uparrow R}^\dagger & c_{\downarrow R}^\dagger \\ ic_{\downarrow R} & -ic_{\uparrow R} \end{pmatrix}. \quad (4)$$

These operators  $U$  have the following commutation rules with the left and right operators

$$\begin{aligned} [U(\vec{y}, \hat{\nu}), R^a(\vec{x}, \hat{\mu})] &= -U(\vec{y}, \hat{\mu}) \frac{\sigma^a}{2} \delta_{\vec{x}\vec{y}} \delta_{\hat{\nu}\hat{\mu}}, \\ [U(\vec{y}, \hat{\nu}), L^a(\vec{x}, \hat{\mu})] &= \frac{\sigma^a}{2} U(\vec{y}, \hat{\mu}) \delta_{\vec{x}\vec{y}} \delta_{\hat{\nu}\hat{\mu}}, \end{aligned} \quad (5)$$

where we have defined the usual Pauli matrices  $\sigma^a$ , see also Ref. [39], while  $\sigma^0$  is defined as the identity operator. The commutation rules for a general gauge transformation follow in a straightforward way,

$$\begin{aligned} \prod_{\vec{y}} e^{-i\theta^a(\vec{y})G^a(\vec{y})} U(\vec{x}, \hat{\mu}) \prod_{\vec{z}} e^{i\theta^a(\vec{z})G^a(\vec{z})} \\ = e^{i\theta^a(\vec{x})(\sigma^a/2)} U(\vec{x}, \hat{\mu}) e^{-i\theta^a(\vec{x}+\hat{\mu})(\sigma^a/2)}, \end{aligned} \quad (6)$$

where the products over  $\vec{y}$  and  $\vec{z}$  are extended over the whole lattice. This equation shows that quantum link models are formulations of gauge-invariant models. In fact, one can notice how the action of a gauge transformation in Eq. (6) mimics Eq. (1).

A generic state in the local Hilbert space  $|n_{\uparrow L}, n_{\downarrow L}, n_{\uparrow R}, n_{\downarrow R}\rangle$  of a quantum link is given by the occupation of the operators  $c_{\uparrow(\downarrow), R(L)}^\dagger$ . Since the total

occupation per link,  $n_{\uparrow L} + n_{\downarrow L} + n_{\uparrow R} + n_{\downarrow R}$ , is a constant of motion [see Eq. (4)], we restrict to the subspace with one occupied mode per link.

Notice that matter-gauge interactions in 1 + 1 dimensions can be derived [39] in a second-order perturbation theory, considering extensions of previous works [50,51]. In the following, we will focus instead on pure-gauge two-dimensional interactions.

*Triangular lattice.*—The continuum limit of quantum link models and their thermodynamical properties are topics under active research. In related condensed matter models, the importance of the lattice geometry has been shown in the fundamental aspect of the phase diagram, as the existence of confinement and deconfinement phases [52,53]. Quantum simulations on large lattices may provide insights on the continuum limit of LGT, and its dependence on the geometry of the underlying lattice. In this spirit, we consider a minimal implementation of a pure SU(2) invariant model in a triangular lattice, by using triangular plaquettes, as depicted in Fig. 1(c). In this case, the pure-gauge Hamiltonian on a single plaquette reads

$$H_T = -J\text{Tr}[U(\vec{x}, \hat{\mu})U(\vec{x} + \hat{\mu}, \hat{\nu})U(\vec{x} + \hat{\mu} + \hat{\nu}, -\hat{\mu} - \hat{\nu})]. \quad (7)$$

This interaction corresponds to the magnetic term of a gauge invariant dynamics, which acts on closed loops. We focus on the magnetic term, since the representation of the electric counterpart is trivial.

Since this Hamiltonian commutes with gauge generators,  $[H_T, G^a(\vec{x})] = 0 \forall \vec{x}, a$ , these are constant of motion, and one can define different gauge sectors with the initial values of the generators. Because of the triangular geometry and having one occupied mode per link, there are no global states that have zero eigenvalue for the gauge generators  $G^a(\vec{x})$  at every vertex in a single plaquette. In general, the absence of the zero-eigenvalue sector depends on the topology of the lattice, and is avoided, for example, in the periodic lattice of Fig. 2(d). The different gauge sectors can be characterized by the eigenvalues of the operator  $\sum_{\vec{x}} \vec{G}^2(\vec{x}) = \sum_{\vec{x}} \sum_a [G^a(\vec{x})]^2$ , as in Figs. 2(a), 2(b), and 2(c); see the Supplemental Material for additional details [39].

The local Hilbert space of a link is four dimensional, and it can be faithfully spanned by two qubits, called “position”  $\sigma_{\text{pos}}^a$  and “spin” qubit  $\sigma_m^a$ . In this subspace, it is useful to define the operators  $\Gamma^0 = \sigma_{\text{pos}}^x \sigma_m^0$ ,  $\Gamma^a = \sigma_{\text{pos}}^y \sigma_m^a$ , such that the total Hamiltonian is written as [39]

$$H_T = -J \left\{ \Gamma_{12}^0 \Gamma_{23}^0 \Gamma_{31}^0 + \sum_{abc} \epsilon_{abc} \Gamma_{12}^a \Gamma_{23}^b \Gamma_{31}^c - \sum_a [\Gamma_{12}^0 \Gamma_{23}^a \Gamma_{31}^a + \Gamma_{12}^a \Gamma_{23}^0 \Gamma_{31}^a + \Gamma_{12}^a \Gamma_{23}^a \Gamma_{31}^0] \right\}. \quad (8)$$

*Superconducting circuit implementation.*—In order to simulate the interaction of Eq. (8), one can decompose its

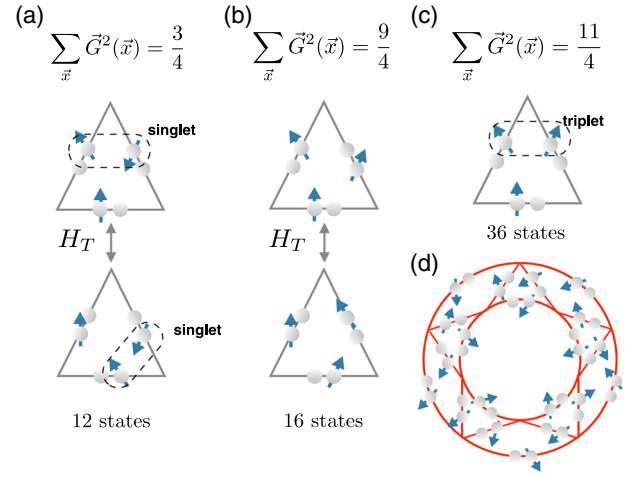


FIG. 2 (color online). (a), (b), and (c) Different gauge invariant sectors for a triangular plaquette, together with the sector degeneracy and the action of the Hamiltonian  $H_T$  upon them. (d) Extended lattice with periodic boundary conditions. This lattice allows for the  $\sum_{\vec{x}} G^2(\vec{x}) = 0$  sector.

dynamics in terms of many-body monomials, and implement them sequentially with a digitized approximation [54]. In a digital approach, one decomposes the dynamics of a Hamiltonian  $H = \sum_{k=1}^m h_k$  by implementing its components stepwise,  $e^{-iHt} \approx (\prod_{k=1}^m e^{-ih_k t/N})^N$  (here and in the following  $\hbar = 1$ ), for a total of  $m \times N$  gates, with an approximation error that goes to zero as the number of repetitions  $N$  grows. In a practical experiment, each quantum gate  $e^{-ih_k t}$  will be affected by a given error  $\epsilon_k$ . By piling up sequences of such gates, for small gate errors  $\epsilon_k \ll 1$ , the total protocol will be affected by a global error, which is approximately the sum  $\epsilon \approx \sum_k \epsilon_k$ . This model for error accumulation has been proved in recent experiments [32,33].

The effects of digitization in the simulation of LGT can be observed in Fig. 3. We have numerically integrated a Schrödinger equation regulated by the Hamiltonian in Eq. (8), choosing as the initial state one of the 12 states shown in Fig. 2(a), for different simulated phases  $\phi = Jt$  [39]. We compute both the evolution with the ideal Hamiltonian and with a digital sequence, in which we act with a single monomial at a time, repeating the protocol  $N$  times. As a figure of merit, we compute the relative deviation  $E = (\langle \sum_{\vec{x}} \vec{G}^2(\vec{x}) \rangle_I - \langle \sum_{\vec{x}} \vec{G}^2(\vec{x}) \rangle_D) / \langle \sum_{\vec{x}} \vec{G}^2(\vec{x}) \rangle_I$  from the ideal value of the gauge invariant, where  $\langle \rangle_{I(D)}$  stand for average values computed on the ideal (digitally simulated) state. The deviation goes to zero for large  $N$  and small phases, defining surfaces at given error tolerance in the  $N - \phi$  space.

To simulate the pure-gauge interaction in a single triangular plaquette, we first consider a setup in which six tunable-coupling transmon qubits are coupled to a single microwave resonator [55,56]. Each tunable-coupling qubit is built using three superconducting islands, connected by two SQUID loops. Acting on these loops with magnetic fluxes, one can modify the coupling of the qubits

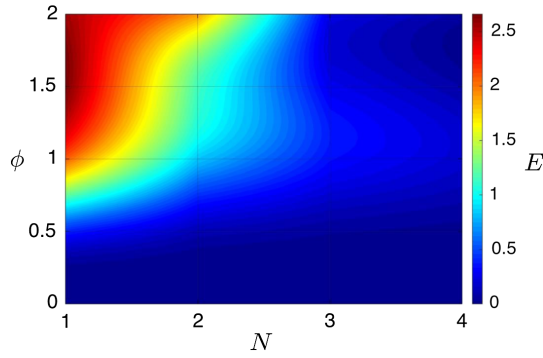


FIG. 3 (color online). The relative gauge deviation of the digitally simulated gauge value  $\langle \rangle_D$ , versus the ideal value  $\langle \rangle_I$ ,  $E = (\langle \sum_{\vec{x}} \vec{G}^2(\vec{x}) \rangle_I - \langle \sum_{\vec{x}} \vec{G}^2(\vec{x}) \rangle_D) / \langle \sum_{\vec{x}} \vec{G}^2(\vec{x}) \rangle_I$ , as a function of the digital steps  $N$  and the simulated phase  $\phi = Jt$ . The error decreases with large  $N$ , and small  $\phi$ . The contour plot is interpolated from numerical data at  $N = \{1, 2, 3, 4\}$ . The initial state is chosen as depicted in Fig. 2(a).

with the resonator, without changing their transition frequencies. For further clarifications of the experimental setup involving tunable-coupling transmon qubits, see the Supplemental Material [39]. By threading with magnetic fluxes at high frequencies, one can drive simultaneous red and blue detuned sidebands, and perform collective gates [57]. Each many-body operator can be realized as a sequence of collective and single-qubit gates,

$$U_N = e^{i(\pi/4) \sum_{i<j} \sigma_i^x \sigma_j^x} e^{i\phi \sigma_i^z} e^{-i(\pi/4) \sum_{i<j} \sigma_i^x \sigma_j^x}, \quad (9)$$

where the indices  $i$  and  $j$  run from 1 to  $N$ . In this way, one can implement a generic (up to  $2N$  local rotations)  $N$ -body evolution operator  $U_N \equiv e^{-i\phi \sigma_1^m \sigma_2^n \dots \sigma_N^k}$ , with  $\{m, n, \dots, k\} \in \{x, y, z\}$ , using 2 collective gates, and a number of single qubit gates, which are upper bounded by  $2N + 1$ , counting the single qubit gate in Eq. (9) and the  $2N$  rotations necessary to map  $U_N$  to any  $N$ -body operator. The simulation for one digital step will amount to implementing 32 collective gates and a number of single qubit gates which are upper bounded by 184 [39].

We consider now the architecture of Fig. 1(b), in which six Xmon qubits in a triangular geometry are capacitively coupled with an additional central ancillary qubit [58]. In this case, the collective interactions  $U_N$  can be decomposed and performed with pairwise controlled-PHASE gates, using the central ancillary qubit to mediate non-nearest interactions. In this way, the quantum simulation of one digital step of the Hamiltonian in Eq. (8) will amount to realize 168 controlled-PHASE gates and a number of single-qubit rotations which are upper bounded by 520. For additional details on the experimental setup and gate counts, see Ref. [39].

To estimate the effects of experimental imperfections on the simulations, we plot in Fig. 4 the dynamics of a single plaquette, starting from a  $\sum_x \vec{G}_x^2 = 9/4$  state. The observed periodic dynamical oscillations between the two paired

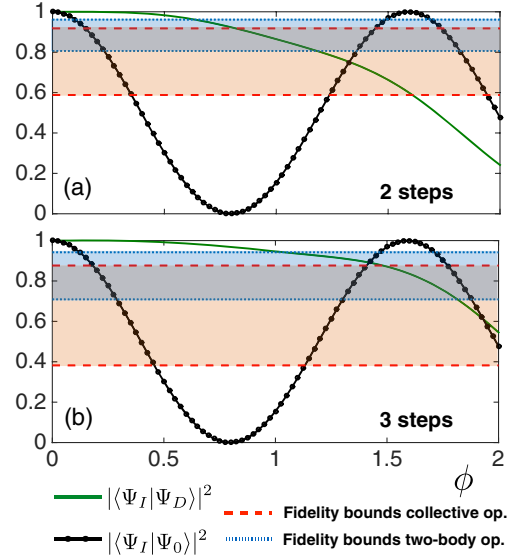


FIG. 4 (color online). Digital quantum simulation of pure gauge dynamics for (a) 2 and (b) 3 digital steps. The initial state  $|\Psi_0\rangle$  is chosen as in Fig. 2(b). Periodic oscillations between the position and qubit degrees of freedom at the vertices are witnessed by  $|\langle \Psi_I | \Psi_0 \rangle|^2$ . The theoretical fidelity  $|\langle \Psi_I | \Psi_D \rangle|^2$  increases with the number of digital steps, together with the width of the fidelity bands due to experimental imperfections.

states, depicted in Fig. 2(b), are signaled by the periodic behavior of the overlap  $|\langle \Psi_I | \Psi_0 \rangle|^2$ . The simulation is run for  $N = 2$  and  $N = 3$  steps, necessary to observe one flip between the two states and one full oscillation, respectively. On top of these oscillations, we plot fidelity bands that estimate the fidelity cap due to accumulated gate errors in the digital protocol, in the case of the two presented setups in Fig. 1, with collective and two-qubit gates. In order to see coherent oscillations, the fidelity of the two-body gates has to be 1 order of magnitude better with respect to the collective ones, with an error window of approximately 0.05%–0.01% in the collective gate case and a 0.005%–0.001% for the controlled-PHASE gate setup. We assume a factor 1/20 for the error loss on a single qubit gate. From the plots, it can be seen that, while the digital fidelity  $|\langle \Psi_I | \Psi_D \rangle|^2$  increases, the fidelity bands due to experimental errors broaden, affecting the simulation. The intersection of the digital fidelity line with the bands marks a regime dominated by experimental imperfections for small  $\phi$ , and one in which the error of the digital expansion prevails for large  $\phi$ .

The proposed simulation can be extended to larger lattices, where one could analyze dynamical properties of the confinement-deconfinement phase transition, which can be traced back to the breaking of the global center symmetry [59] in groups with a nontrivial center group, like the SU(2) case. Moreover, such a LGT simulator can be used to perform quench experiments in a ladder configuration, analyzing breaking of gluon strings between pairs of particles and antiparticles [60–62].

In order to scale the quantum simulation to large qubit lattices, one has to consider that the accumulated gate error does not depend on the size of the lattice [32,33], and only on the number of gates. The quantum resources necessary to run the simulation scale polynomially in the lattice size, and subpolynomially in the digital error [63], making the whole protocol efficient. With a current total number of gates that exceeds 1000 [32,34], we believe that in the near future simulations of LGT on large scales will be feasible. Furthermore, the possibility of performing quantum error correction for digital quantum simulations may drastically increase its effectiveness [64].

A. M. and L. L. acknowledge useful discussions with Rami Barends. E. R. thanks D. Banerjee, T. Calarco, M. Dalmonte, S. Montangero, U.-J. Wiese, and P. Zoller for discussions, in the framework of quantum technologies for lattice gauge theories. We acknowledge financial support from Basque Government Grants No. IT472-10 and No. IT559-10, Spanish MINECO FIS2012-36673-C03-02, Ramón y Cajal Grant RYC-2012-11391, UPV/EHU Project No. EHUA14/04, UPV/EHU UFI 11/55, PROMISCE, and SCALEQIT European projects.

- 
- [1] I. Montvay and G. Münster, *Quantum Fields on a Lattice* (Cambridge University Press, Cambridge, England, 1994).
- [2] H. J. Rothe, *Lattice Gauge Theories* (World Scientific, Singapore, 2012).
- [3] I. Affleck, Z. Zou, T. Hsu, and P. W. Anderson, *Phys. Rev. B* **38**, 745 (1988).
- [4] E. Dagotto, E. Fradkin, and A. Moreo, *Phys. Rev. B* **38**, 2926 (1988).
- [5] X. G. Wen, *Quantum Field Theory of Many-Body Systems: From the Origin of Sound to an Origin of Light and Electrons*, (Oxford Graduate Texts, Oxford, 2004).
- [6] K. G. Wilson, *Phys. Rev. D* **10**, 2445 (1974).
- [7] J. Kogut and L. Susskind, *Phys. Rev. D* **11**, 395 (1975).
- [8] S. Durr, Z. Fodor, J. Frison, C. Hoelbling, R. Hoffmann, S. D. Katz, S. Krieg, T. Kurth, L. Lellouch, T. Lippert, K. K. Szabo, and G. Vulvert, *Science* **322**, 1224 (2008).
- [9] R. P. Feynman, *Int. J. Theor. Phys.* **21**, 467 (1982).
- [10] H. Weimer, M. Müller, I. Lesanovsky, P. Zoller, and H. P. Buchler, *Nat. Phys.* **6**, 382 (2010).
- [11] E. Kapit and E. Mueller, *Phys. Rev. A* **83**, 033625 (2011).
- [12] E. Zohar and B. Reznik, *Phys. Rev. Lett.* **107**, 275301 (2011).
- [13] E. Zohar, J. I. Cirac, and B. Reznik, *Phys. Rev. Lett.* **109**, 125302 (2012).
- [14] D. Banerjee, M. Dalmonte, M. Müller, E. Rico, P. Stebler, U.-J. Wiese, and P. Zoller, *Phys. Rev. Lett.* **109**, 175302 (2012).
- [15] E. Zohar, J. I. Cirac, and B. Reznik, *Phys. Rev. Lett.* **110**, 055302 (2013).
- [16] L. Tagliacozzo, A. Celi, A. Zamora, and M. Lewenstein, *Ann. Phys. (Berlin)* **330**, 160 (2013).
- [17] E. Zohar, J. I. Cirac, and B. Reznik, *Phys. Rev. A* **88**, 023617 (2013).
- [18] D. Marcos, P. Widmer, E. Rico, M. Hafezi, P. Rabl, U.-J. Wiese, and P. Zoller, *Ann. Phys. (Berlin)* **351**, 634 (2014).
- [19] K. Stannigel, P. Hauke, D. Marcos, M. Hafezi, S. Diehl, M. Dalmonte, and P. Zoller, *Phys. Rev. Lett.* **112**, 120406 (2014).
- [20] A. W. Glaetzle, M. Dalmonte, R. Nath, I. Roussochatzakis, R. Moessner, and P. Zoller, *Phys. Rev. X* **4**, 041037 (2014).
- [21] S. Notarnicola, E. Ercolessi, P. Facchi, G. Marmo, S. Pascazio, and F. V. Pepe, *J. Phys. A* **48**, 30FT01 (2015).
- [22] A. Bazavov, Y. Meurice, S.-W. Tsai, J. Unmuth-Yockey, and J. Zhang, *Phys. Rev. D* **92**, 076003 (2015).
- [23] L. Tagliacozzo, A. Celi, P. Orland, and M. Lewenstein, *Nat. Commun.* **4**, 2615 (2013).
- [24] D. Banerjee, M. Bögli, M. Dalmonte, E. Rico, P. Stebler, U.-J. Wiese, and P. Zoller, *Phys. Rev. Lett.* **110**, 125303 (2013).
- [25] E. Zohar, J. I. Cirac, and B. Reznik, *Phys. Rev. Lett.* **110**, 125304 (2013).
- [26] U.-J. Wiese, *Nucl. Phys. A* **931**, 246 (2014).
- [27] E. Zohar, J. Cirac, and B. Reznik, *arXiv:1503.02312*.
- [28] I. M. Georgescu, S. Ashhab, and F. Nori, *Rev. Mod. Phys.* **86**, 153 (2014).
- [29] M. H. Devoret and R. Schoelkopf, *Science* **339**, 1169 (2013).
- [30] U. Las Heras, A. Mezzacapo, L. Lamata, S. Filipp, A. Wallraff, and E. Solano, *Phys. Rev. Lett.* **112**, 200501 (2014).
- [31] U. Las Heras, L. García-Álvarez, A. Mezzacapo, E. Solano, and L. Lamata, *EPJ Quantum Technology* **2**, 8 (2015).
- [32] R. Barends, L. Lamata, J. Kelly, L. García-Álvarez, A. G. Fowler, A. Megrant, E. Jeffrey, T. C. White, D. Sank, J. Y. Mutus, B. Campbell, Y. Chen, Z. Chen, B. Chiaro, A. Dunsworth, I.-C. Hoi, C. Neill, P. J. J. O'Malley, C. Quintana, P. Roushan, A. Vainsencher, J. Wenner, E. Solano, and J. M. Martinis, *Nat. Commun.* **6**, 7654 (2015).
- [33] Y. Salathé, M. Mondal, M. Oppliger, J. Heinsoo, P. Kurpiers, A. Potočnik, A. Mezzacapo, U. Las Heras, L. Lamata, E. Solano, S. Filipp, and A. Wallraff, *Phys. Rev. X* **5**, 021027 (2015).
- [34] R. Barends *et al.*, *arXiv:1511.03316*.
- [35] B. P. Lanyon, C. Hempel, D. Nigg, M. Müller, R. Gerritsma, F. Zähringer, P. Schindler, J. T. Barreiro, M. Rambach, G. Kirchmair, M. Hennrich, P. Zoller, R. Blatt, and C. F. Roos, *Science* **334**, 57 (2011).
- [36] J. Casanova, A. Mezzacapo, L. Lamata, and E. Solano, *Phys. Rev. Lett.* **108**, 190502 (2012).
- [37] A. Mezzacapo, J. Casanova, L. Lamata, and E. Solano, *Phys. Rev. Lett.* **109**, 200501 (2012).
- [38] R. Brower, S. Chandrasekharan, and U.-J. Wiese, *Phys. Rev. D* **60**, 094502 (1999).
- [39] See Supplemental Material at <http://link.aps.org/supplemental/10.1103/PhysRevLett.115.240502> for additional analysis and computational details, which includes Refs. [40–46].
- [40] V. Bouchiat, D. Vion, P. Joyez, D. Esteve, and M. H. Devoret, *Phys. Scr.* **T76**, 165 (1998).
- [41] A. Blais, R.-S. Huang, A. Wallraff, S. M. Girvin, and R. J. Schoelkopf, *Phys. Rev. A* **69**, 062320 (2004).

- [42] A. Wallraff, D. I. Schuster, A. Blais, L. Frunzio, R.-S. Huang, J. Majer, S. Kumar, S. M. Girvin, and R. J. Schoelkopf, *Nature (London)* **431**, 162 (2004).
- [43] J. Koch, T. M. Yu, J. Gambetta, A. A. Houck, D. I. Schuster, J. Majer, A. Blais, M. H. Devoret, S. M. Girvin, and R. J. Schoelkopf, *Phys. Rev. A* **76**, 042319 (2007).
- [44] M. Müller, K. Hammerer, Y. L. Zhou, C. F. Roos, and P. Zoller, *New J. Phys.* **13**, 085007 (2011).
- [45] J. M. Martinis and M. R. Geller, *Phys. Rev. A* **90**, 022307 (2014).
- [46] M. Suzuki, *Phys. Lett. A* **146**, 319 (1990).
- [47] D. Horn, *Phys. Lett.* **100B**, 149 (1981).
- [48] P. Orland and D. Rohrlich, *Nucl. Phys.* **B338**, 647 (1990).
- [49] M. Mathur, *J. Phys. A* **38**, 10015 (2005).
- [50] P. Hauke, D. Marcos, M. Dalmonte, and P. Zoller, *Phys. Rev. X* **3**, 041018 (2013).
- [51] D. Marcos, P. Rabl, E. Rico, and P. Zoller, *Phys. Rev. Lett.* **111**, 110504 (2013).
- [52] D. S. Rokhsar and S. A. Kivelson, *Phys. Rev. Lett.* **61**, 2376 (1988).
- [53] R. Moessner and S. L. Sondhi, *Phys. Rev. Lett.* **86**, 1881 (2001).
- [54] S. Lloyd, *Science* **273**, 1073 (1996).
- [55] J. M. Gambetta, A. A. Houck, and A. Blais, *Phys. Rev. Lett.* **106**, 030502 (2011).
- [56] S. J. Srinivasan, A. J. Hoffman, J. M. Gambetta, and A. A. Houck, *Phys. Rev. Lett.* **106**, 083601 (2011).
- [57] A. Mezzacapo, L. Lamata, S. Filipp, and E. Solano, *Phys. Rev. Lett.* **113**, 050501 (2014).
- [58] R. Barends, J. Kelly, A. Megrant, D. Sank, E. Jeffrey, Y. Chen, Y. Yin, B. Chiaro, J. Mutus, C. Neill, P. O'Malley, P. Roushan, J. Wenner, T. C. White, A. N. Cleland, and J. M. Martinis, *Phys. Rev. Lett.* **111**, 080502 (2013).
- [59] J. Greensite, *An Introduction to the Confinement Problem*, Springer, Lecture Notes in Phys. (Springer, New York, 2011), Vol. 821.
- [60] M. Pepe and U.-J. Wiese, *Phys. Rev. Lett.* **102**, 191601 (2009).
- [61] S. Kühn, J. I. Cirac, and M. C. Bañuls, *J. High Energy Phys.* **07** (2015) 130.
- [62] T. Pichler, M. Dalmonte, E. Rico, P. Zoller, and S. Montangero, [arXiv:1505.04440](https://arxiv.org/abs/1505.04440).
- [63] D. W. Berry, G. Ahokas, R. Cleve, and B. C. Sanders, *Commun. Math. Phys.* **270**, 359 (2007).
- [64] R. Barends, J. Kelly, A. Megrant, A. Veitia, D. Sank, E. Jeffrey, T. C. White, J. Mutus, A. G. Fowler, B. Campbell, Y. Chen, Z. Chen, B. Chiaro, A. Dunsworth, C. Neill, P. O. Malley, P. Roushan, A. Vainsencher, J. Wenner, A. N. Korotkov, A. N. Cleland, and J. M. Martinis, *Nature (London)* **508**, 500 (2014).